ADVANCED FUNCTIONAL MATERIALS
www.afm-journal.de

www.MaterialsViews.com

Blue–Green Emission in Terbium-Doped Alumina (Tb:Al_2O_3) Transparent Ceramics

*Elias H. Penilla, Yasuhiro Kodera, and Javier E. Garay**

Alumina (Al_2O_3) is one of the most versatile ceramics, utilized in an amazing range of structural and optical applications. In fact, chromium-doped single crystal Al_2O_3 was the basis for the first laser. Today, most photoluminescent (PL) materials rely on rare earth (RE) rather than transition-metal dopants because RE doping produces greater efficiencies and lower lasing thresholds. RE-doped alumina could provide an extremely versatile PL ceramic, opening the door for a host of new applications and devices. However, producing a transparent RE:Al_2O_3 suitable for PL applications is a major challenge due to the very low equilibrium solubility of RE (~10^{-3}%) in Al_2O_3 in addition to alumina's optical anisotropy. A method is presented here to successfully incorporate Tb^{3+} ions up to a concentration of 0.5 at% into a dense alumina matrix, achieving a transparent light-emitting ceramic. Sub-micrometer alumina and nanometric RE oxide powders are simultaneously densified and reacted using current-activated, pressure-assisted densification (CAPAD), often called spark plasma sintering (SPS). These doped ceramics have a high transmission (~75% at 800 nm) and display PL peaks centered at 485 nm and 543 nm, characteristic of Tb^{3+} emission. Additionally, the luminescent lifetimes are long and compare favorably with lifetimes of other laser ceramics. The high transparencies and PL properties of these ceramics have exciting prospects for high energy laser technology.

1. Introduction

Although functional transparent polycrystalline ceramics have been studied for decades[1,2] their continued development as an alternate or replacement for single crystal optical materials remains intense.[3] The allure is twofold, first polycrystalline ceramics are often more efficiently manufactured and second it is possible to fabricate bulk ceramics in compositions that simply cannot be made as single crystals. The first impetus is exemplified by the development of polycrystalline neodymium doped yttrium aluminum garnet (Nd:YAG) to a point where they have lasing slope efficiencies on par with single crystal variants.[4,5] The second incentive stems from the fact that single crystal manufacturing methods such as the Czochralski and Verneuill techniques are bound by thermodynamic equilibrium which limits possible crystal structures and dopant concentrations. On the other hand, certain polycrystalline ceramic preparation techniques offer the flexibility of producing compounds not dictated by equilibrium.

Of particular interest is current-activated pressure-assisted densification (CAPAD) that employs very high heating rates and thus can potentially operate far from equilibrium.[6] One major driver for the search for single crystal replacement has been in finding laser host materials for tomorrow's high power lasers.[7–9] Currently, the relatively low thermal conductivity of the state of the art host material, yttrium aluminum garnet (YAG) is the bottleneck for the development of higher power and/or higher duty-cycle solid state lasers. This is because low thermal conductivity causes high thermal gradients in the material as it is pumped and consequentially degrades the beam quality. Thus the power deliverable by a laser directly scales with the thermal conductivity for a given pumping/cooling scheme. In response researchers have been working on developing gain materials with higher thermal conductivities than YAG,[10,11] (YAG has thermal conductivities between 9 to 14 W m^{-1} K^{-1}).[12,13] Notable examples are Y_2O_3[14] and Sc_2O_3,[14,15] which have been shown to have thermal conductivities of ~17 W m^{-1} K^{-1} in polycrystalline form. An even greater improvement in thermal conductivity and therefore device power could be achieved by using alumina (Al_2O_3) as a rare earth host; alumina has a single crystal conductivity between 32 and 35 W m^{-1} K^{-1} at room temperature,[16] representing a possible doubling in the peak output power, duty cycle, or compactness of a laser system when comparing to state of the art lasing media.

There are several major hurdles to producing transparent polycrystalline alumina doped with rare earths (RE) for photonic functionalization. The first is that alumina has a hexagonal symmetry and is birefringent so that there is significant scatter at grain boundaries in polycrystalline materials. This problem can be solved by producing ceramics with relatively fine average grain size (AGS). Several researchers including the groups of Klimke[17] and van Bruggen[18] have demonstrated highly transparent polycrystalline Al_2O_3 with sub-micrometer AGS. The second and more difficult problem is the very low RE equilibrium solubility in alumina, which is ~10^{-3} at%,[19] a

E. H. Penilla, Dr. Y. Kodera, Prof. J. E. Garay
Advanced Materials Processing and Synthesis (AMPS) Laboratory
Department of Mechanical Engineering, Materials Science and Engineering Program
University of California
Riverside, CA, 92521, USA
E-mail: jegaray@engr.ucr.edu

DOI: 10.1002/adfm.201300906

Table 1. Processing parameters and properties of the CAPAD produced ceramics

Sample	Dopant [at%Tb]	Temp. [°C]	Heating rate [°C min^{-1}]	Hold time [min]	Relative density [%]	Average grain size ± std. dev. [nm]	Transmittance @ λ > 950 nm [%]	FWHM of 489 nm PL peak [nm]	FWHM of 543 nm PL peak [nm]
1	0	1200	300	10	>99	340 ± 1 0	83	N/A	N/A
2	0.5	1200	150	10	>99	242 ± 69	81	14	11
3	0.5	1200	300	10	>99	232 ± 63	83	14	12
4	0.5	1200	600	10	>99	256 ± 56	82	16	12
5	0.5	1200	300	20	>99	348 ± 110	81	15	12
6	0.5	1200	300	30	>99	375 ± 100	80	15	13

concentration too low for efficient light production; RE levels greater than 0.1 at% are typical in ruby[20] and RE:YAG[21] based devices. This requirement indicates that at least a 100 fold higher than equilibrium dopant concentration is needed to make a RE:Al_2O_3 ceramic a viable laser host material. The limitation imposed by processing under conditions dictated by thermodynamic equilibrium precludes the use of the single crystal growing, as well as traditional sintering techniques that are the standard for producing optical quality alumina ceramics.[22]

In order to achieve the elusive goal of producing rare-earth doped alumina ceramics suitable for laser applications, a material processing technique is needed that can deliver the proper control of microstructure (fine grains and very low porosity), ensuring high transparency, and can operate out of thermodynamic equilibrium conditions, so that a higher functional level of RE-dopant concentration can be achieved. Here we present a method for the successful incorporation of Tb^{3+} ions to a concentration as high as 0.5 at% relative to the Al^{3+} ion, into a sub-micron highly dense alumina matrix, resulting in a transparent, visible light emitting ceramic.

The transparencies of our Tb^{3+} doped alumina (Tb:Al_2O_3) ceramics approach the single-crystal limit for alumina of ~86% and the dopant concentration of 0.5 at% represents a 500 fold improvement over the concentrations achievable by traditional techniques bound by thermodynamic equilibrium, surpassing the requisite metric for laser operation mentioned above by a factor of 5. Our method relies on the simultaneous densification and reaction of sub-micron alumina powder along with rare earth oxides as a photoluminescent source using CAPAD. To the best of our knowledge, this is the first time a birefringent (non-cubic) polycrystalline oxide bulk ceramic has been shown to possess both high transparency and RE induced light emission properties. The high transparency and photoluminescent properties associated with the high RE-dopant concentration of our samples indicate that these materials are promising candidates for photonic applications such as laser host ceramics. In particular the higher thermal conductivity of these ceramics enables the doubling of peak power, duty cycle, or the compactness of the laser system can be increased in comparison with state of the art laser host ceramics.

2. Results and Discussion

Commercial Al_2O_3 and Tb_4O_7 powders were mixed and prepared for CAPAD processing (see Experimental Section for details). The CAPAD processing parameters we used are tabulated in **Table 1**. In order to produce non-cubic (i.e. materials that can be birefringent) transparent polycrystalline ceramics, such as polycrystalline alumina, it is imperative to minimize the sample porosity and maintain a fine grain size. Since pores are very efficient scattering sites,[23] low porosity decreases light scattering and maintaining the AGS below 1–2 μm in diameter minimizes the effects of birefringence related scattering in alumina.[18] The effect of CAPAD processing temperature on the density of alumina and 0.5 at% Tb^{3+} doped alumina (Tb:Al_2O_3) samples is shown in **Figure 1**. As expected, density increases with temperature in both Tb^{3+} doped and un-doped cases. At low and intermediate temperatures, the doped samples have a lower relative density than the un-doped case. We have observed this phenomena in another rare earth doped cerami.[24] We attribute the observed lower densities to dopant atoms decreasing the densification rate, likely by inhibiting particle sliding and/or grain boundary diffusion. Both un-doped and doped samples reach near-full density, >99% relative density at temperatures of 1200 °C.

Figure 2 shows pictures of un-doped (Figure 2a) and doped (Figure 2b) samples produced at 1200 °C. The printed lettering

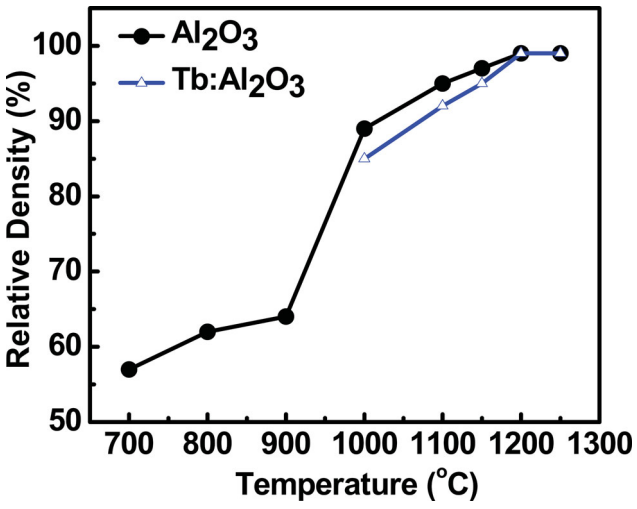

Figure 1. The effect of processing temperature on the relative density of un-doped alumina (Al_2O_3) and 0.5 at% Tb doped alumina (Tb:Al_2O_3). The samples were all processed using a pressure of 105 MPa, 300 °C min^{-1} heating rate, and held at the temperature indicated for 10 min.

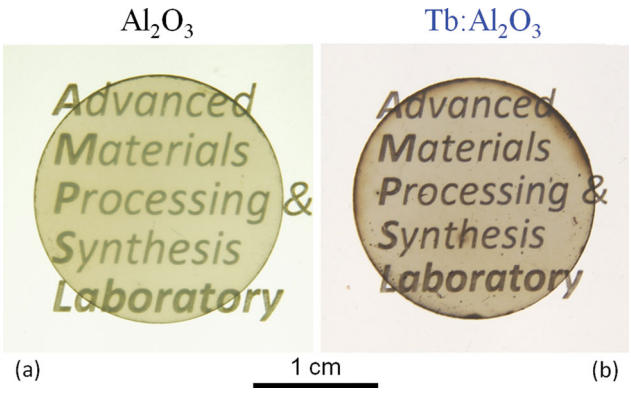

Figure 2. Photographs of CAPAD processed ceramics on back lit text. The samples were processed using 1200 °C, 105 MPa, 300 °C min^{-1} heating rate and 10 min hold time. The samples are 19 mm in diameter and 1 mm thick. The printed text below the sample is legible demonstrating the transparency of the ceramics. (a) Un-doped alumina (Al_2O_3) ceramic (b) 0.5 at% Tb^{3+} doped alumina ($Tb:Al_2O_3$).

is visible through the ceramic disks demonstrating good transparency. The high transparency of our ceramics is attributed to the high relative density and fine average grain size of our ceramics which are listed in Table 1. The AGS was determined by measuring approximately 500 grains from multiple fracture surface scanning electron microscope (SEM) micrographs of each sample (for further details please refer to the experimental techniques section). Representative SEM fracture surfaces are presented in **Figure 3** for the Al_2O_3 and $Tb:Al_2O_3$ samples produced at various heating rate (HR) with constant hold time (HT). The SEM micrographs do not show evidence of residual porosity, which corroborates the high density measurements reported in Figure 1. It is possible that low concentrations of very fine diameter pores are present but are difficult to detect with SEM.

The un-doped Al_2O_3 sample produced at 1200 °C, with a heating rate (HR) of 300 °C min^{-1}, and a 10 min hold time (HT) has an AGS of ~340 nm with a standard deviation of ~10 nm, indicating a very homogenous fine grained microstructure with minimal grain growth (the starting powder crystallite size is ~150–250 nm). The AGS of the $Tb:Al_2O_3$ samples produced at the same temperature and HT with varying HR are smaller than in the un-doped case; the AGS is approximately 250 nm ± 50–60 nm. We observe no strong trend with respect to the HR. The smaller AGS can be indicative of a grain boundary pinning effect associated with dopant segregation at the grain boundary, an effect similar to that seen when MgO is used as a sintering additive for alumina ceramic.[1] Such grain boundary pinning likely occurs at the early stages of reaction-densification when the Al_2O_3 and Tb_4O_7 phases are still separate phases. This coupled with the short processing times associated with CAPAD explain the minimal grain growth in these $Tb:Al_2O_3$ samples. The effect of HT on the resultant microstructure followed the usual trend, i.e. increasing the HT to 20 and 30 min with all other parameters held constant results in an increased AGS of ~348 ± 110 nm and of ~375 ± 100 nm, respectively.

The high transparency of the samples over the entire visible range (400–800 nm) as well as the UV and NIR can be quantitatively appreciated in **Figure 4** which shows the percent total transmission as a function of wavelength for un-doped and doped alumina produced using identical processing conditions. The values were corrected to account for reflectance losses at the front and back polished sample surfaces,

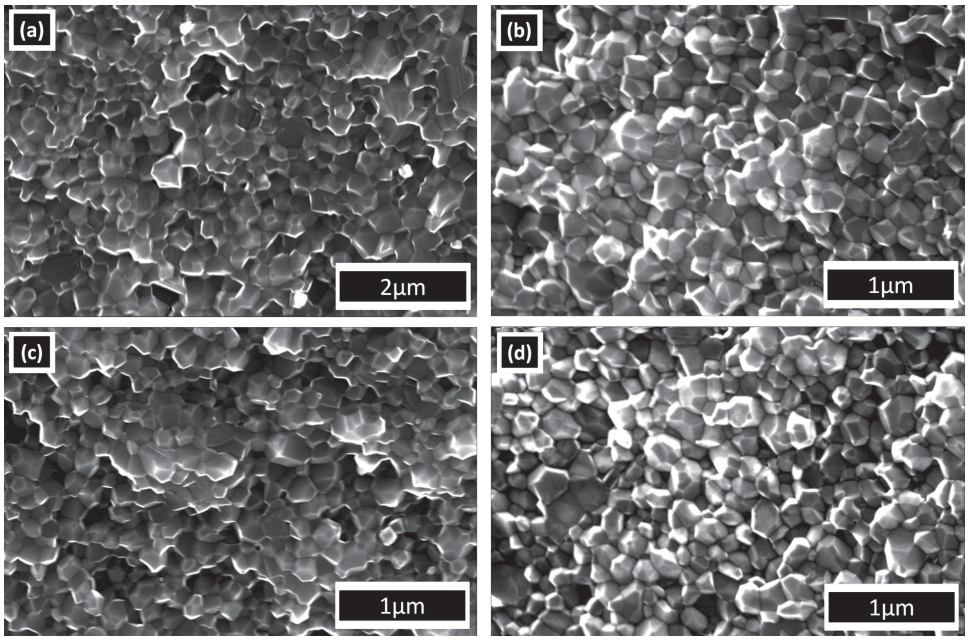

Figure 3. Representative Fracture Surface SEMs for the un-doped Al_2O_3 and $Tb:Al_2O_3$ samples produced at 1200 °C, 105 MPa, and with a 10 min hold time, with various heating rates (HR), where (a) Un-doped Al_2O_3, (b) $Tb:Al_2O_3$, HR = 150 °C min^{-1}, (c) $Tb:Al_2O_3$, HR = 300 °C min^{-1}, and (d) $Tb:Al_2O_3$, HR = 600 °C min^{-1}.

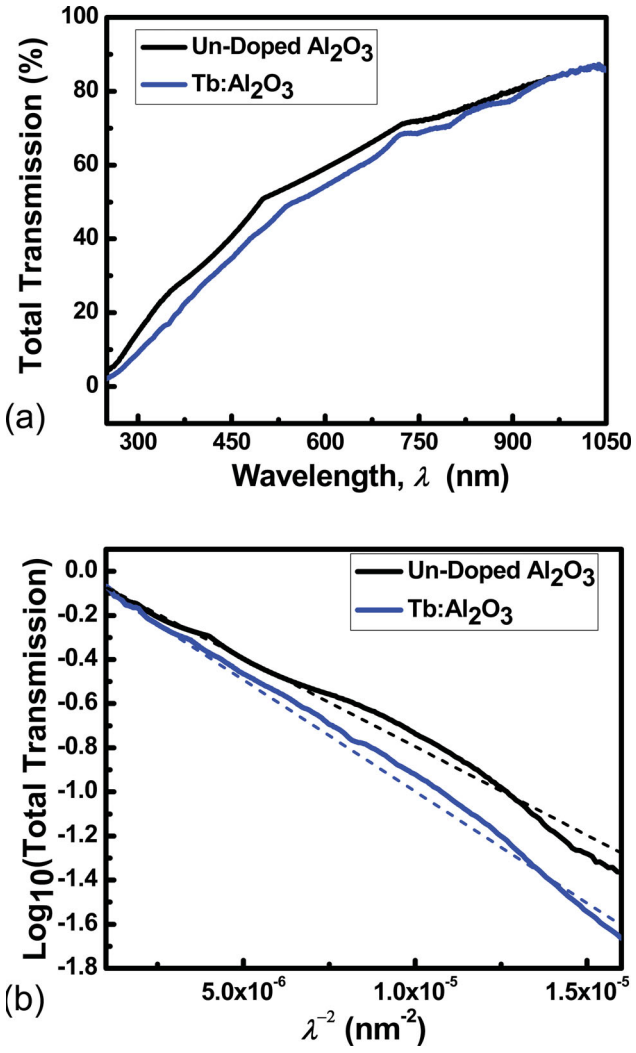

Figure 4. (a) Total transmission versus wavelength for doped (Tb:Al_2O_3) and un-doped alumina (Al_2O_3) ceramics. The processing parameters were held constant (1200 °C, 105 MPa, 300 °C min^{-1} heating rate and 10 min hold time). (b) The same data as in Figure 3a, plotted as the logarithm of the total transmission versus $1/\lambda^2$. The dashed lines are straight lines, demonstrating the good linear fit of the data.

assuming a reflectance of 14%, based on the refractive index of polycrystalline alumina.[18] In both cases the transparency increases with wavelength from the UV through the VIS and into the NIR. The un-doped alumina has slightly higher transmission below ~775 nm than the Tb:Al_2O_3 samples; at higher wavelengths the transparencies are quite similar. These results reveal that both Al_2O_3 and Tb:Al_2O_3 ceramics have a transparency of ~75% at the edge of the visible (800 nm) and actually reach ~83% total transmission at $\lambda > 950$ nm, approaching the maximum theoretical transparency for single crystal sapphire (~86%).[18] These are impressive transparencies for polycrystalline ceramics especially in a birefringent material.

Pecharromán et al.,[25] following a similar approach to Apetz and Van Bruggen,[18] applied the Rayleigh-Gans-Debye (RGD) approximation in order to analyze the optical transparency in alumina with small grain sizes. They derive the following expression that relates the real in line transmission, T with microstructural parameters and wavelength, λ as:

$$\log(T) = \log(T_0) - \frac{6\pi^2 \langle a_g \rangle}{\lambda^2} \Delta n^2 a d \quad (1)$$

where $\langle a_g \rangle$ is the maximum grain size, Δn is the change in refractive index (birefringence), α is texture parameter and d is the sample thickness. In Figure 4b, we plot the transmission results shown in Figure 4a as $\log(T)$ vs. $1/\lambda^2$. The dashed lines are straight lines showing the good linear fit of the transmission curves. The good fit to Equation (1) indicates that the consolidated ceramics possess a relatively fine grain size, i.e. the grain size of the ceramics is comparable to the incident wavelength. They also indicate that there is not significant scattering from residual porosity; a $1/\lambda^4$ relationship would be expected if significant porosity were present. The results in Figure 4b are consistent with our measured AGS of less than 400 nm as discussed above and they also corroborate our lack of observable residual porosity in the fracture surface SEM.

In addition to being highly transparent, the doped ceramics display photoluminescence (PL). The strong (a quantitative analysis of the PL will be presented below) visible fluorescence of the Tb:Al_2O_3 sample when exposed to UV light can be appreciated in **Figure 5**. Figure 5 shows pictures of un-doped Al_2O_3 and Tb:Al_2O_3 samples subjected to a 355 nm pulsed laser with a 0.5 cm diameter spot size. The pictures are top-views of the ceramics where the laser light is incident on the back of the ceramic. The pictures were taken in a darkened room so that ambient light would not overwhelm the possible luminescence from the samples. The un-doped sample shows a very faint color near the center where the 355 nm is transmitted through the sample. The rest of the sample is dark as expected since it does not display luminescence. The difference when the Tb:Al_2O_3 is exposed to UV light is dramatic. The picture (Figure 5b) clearly shows a bright green spot where the 355 nm pulsed laser is incident on the sample. In addition there is also

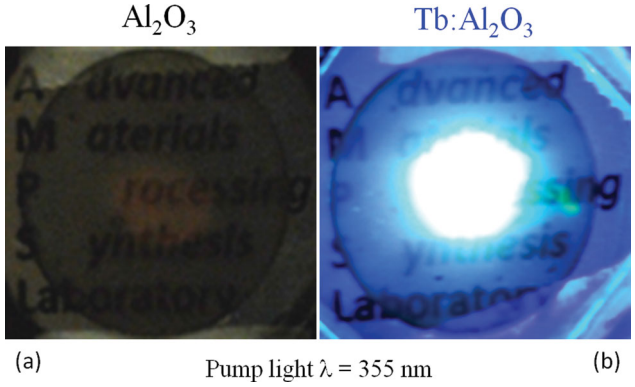

Figure 5. Photographs of CAPAD processed ceramics being exited with 355 nm UV pulsed laser light. The laser light is incident on the back of the samples. The samples were processed using 1200 °C, 105 MPa, 300 °C min^{-1} heating rate and 10 min hold time. (a) Un-doped alumina. The sample does not photoluminescence causing the picture to be dark. The incident UV light is barely visible near the center of the sample. (b) Tb:Al_2O_3 alumina. The picture clearly shows blue and green photoluminescence of the ceramic caused by UV (355 nm) excitation.

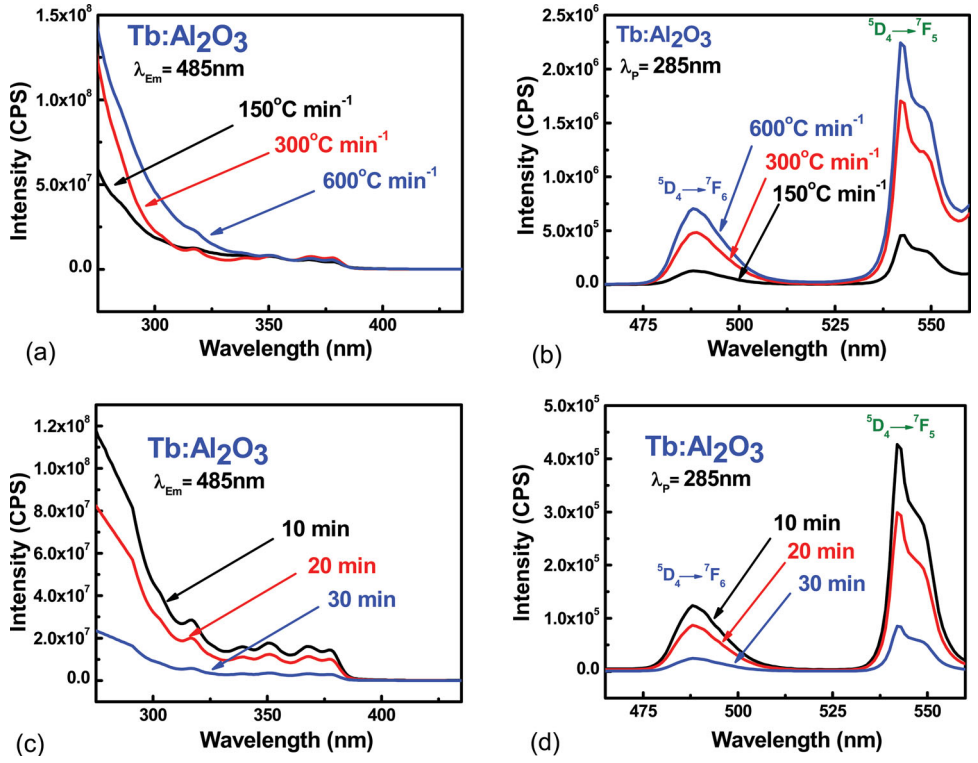

Figure 6. Excitation and emission scans of Tb:Al_2O_3 produced using varying processing conditions (heating rate or hold time). The processing temperature and pressure were held constant, 1200 °C and 105 MPa. The Excitation Scans were taken monitoring at 485 nm (λ_{Em} = 485 nm) and the emission scans were taken using 285 nm illumination (λ_P = 285 nm). The emission scans reveal two sharp PL peaks corresponding to the $^5D_4 \rightarrow {}^7F_6$ and $^5D_4 \rightarrow {}^7F_5$ transitions of Tb^{3+} ion (a) Excitation scan of Tb:Al_2O_3 produced using varying heating rates and constant hold time, 10 min. (b) Emission scan of Tb:Al_2O_3 produced using varying heating rates and constant hold time, 10 min. (c) Excitation scan of Tb:Al_2O_3 produced using varying hold time and constant heating rate 300 °C min^{-1}. (d) Emission scan of Tb:Al_2O_3 produced using varying hold time and constant heating rate 300 °C min^{-1}.

a blue halo visible around the sample. It is worth emphasizing that since the incident UV light is not visible, all of the blue-green light visible in Figure 5b is coming from the sample. As will be discussed in further detail below, the PL spectra **Figure 6** reveals that the Tb:Al_2O_3 ceramics produce two distinct PL peaks, one at 485 nm which should appear blue while the second at 543 nm should appear green. The mixing of these two peaks explains the blue-green appearance of the PL in Figure 5.

Figure 6 shows excitation and emission scans of Tb:Al_2O_3 ceramics produced using different processing conditions. The measurements shown in Figure 6a and b were for samples produced using 3 different HR, 150, 300 and 600 °C min^{-1} with the same HT of 10 min and temperature, 1200 °C. The spectra shown in Figure 6c and d were taken from samples produced with varying HT keeping the HR constant at 300 °C min^{-1} and maximum process temperature of 1200 °C. The excitation scans (Figure 6a,c) were taken by monitoring the 485 nm peak and show that UV excitation below ~375 nm can be used to produce significant luminescence at 485 nm. The emission scans of the Tb:Al_2O_3 (Figure 6b,d) show two distinct sharp luminescence peaks. These peaks correspond to the $^5D_4 \rightarrow {}^7F_6$ transition centered on 485 nm and the $^5D_4 \rightarrow {}^7F_5$ transition centered at 543 nm. These transitions corresponding to Tb^{3+} were labeled according to the Dieke diagram.[26] These spectra confirm that Tb^{3+} dopants were successfully incorporated into the alumina matrix. We attribute the successful incorporation of Tb^{3+} to the increased processing kinetics offered by the CAPAD process. We have previously shown that high HR in CAPAD processing can promote rapid diffusion and drastically increase processing kinetics when compared to free sintering[24] in another oxide system. The increased diffusion and processing kinetics of CAPAD processing allow for higher than equilibrium rare-earth dopant concentration. The heating rates of 150–600 °C min^{-1} for this work is significantly higher than the HR associated with free sintering and hot pressing, which are typically on the order of 10 °C min^{-1} to 50 °C min^{-1}.

Similarly the cooling rate (CR) of our process is about 300 °C min^{-1} which is again substantially higher than CR's for free sintering and hot pressing (typically <5 °C min^{-1}), because most furnaces and hot presses are heavily insulated and tend to rely only on convection for cooling. These high CR allow the 'freezing-in' of the higher than equilibrium concentration of Tb^{3+}. It should be noted that although these ceramics have higher RE-dopant concentrations than the equilibrium solubility limit there is little chance that dopant segregation will occur in applications. The typical operation temperatures of devices such as solid state lasers are never more than ~200 °C, a temperature at which the diffusivity of Tb^{3+} ions would be prohibitively low.

Interestingly, the heating rate used during CAPAD processing plays a significant role on the PL intensity of the

samples; higher heating rates produce higher intensity from both peaks as can be seen in Figure 6b. For example, in the $^5D_4 \rightarrow {}^7F_6$ transition centered around 485 nm, increasing the HR from 150 °Cmin^{-1} to 300 °C min^{-1} and 600 °C min^{-1} results in a ~1.5 and ~5.5 increase in the PL output intensity, respectively (at the same pumping intensity). Similarly for the $^5D_4 \rightarrow {}^7F_5$ transition centered at 543 nm, the same increases in HR results in increased PL intensities by factors of ~1.3 and ~4.9, respectively. These measurements indicate that varying HR during CAPAD processing affects the relative efficiencies of the Tb:Al_2O_3 transparent ceramics. Since the pumping intensity is the same in all instances, this indicates that using a higher HR can cause as much as a five-fold increase in the relative efficiency of these materials.

An increase in PL intensity can be caused by decreased scattering, absorption or a change in electron environment around the luminescent ion. One possibility for the observed dependence of PL intensity on HR is that varying HR causes varying levels of residual stress or distortion of the lattice around the active Tb^{3+} ions. However, comparison of the full width at half the maximum value (FWHM) (Table 1) of the PL peaks shows that they are all very similar suggesting similar electronic environment near the Tb^{3+} ions. Measurements of residual stress in sintered alumina by Krell[27] et al. show that although residual stress levels in alumina are grain size dependent due to an anisotropic (hexagonal) crystal structure, they reach a plateau in small grained samples and thus remain similar in alumina with sub-micron grains. Since our ceramics have an AGS < 400 nm, at all HR's, the residual stress levels are also likely to be independent of HR, which is consistent with our observation that the FWHM values of the PL peaks are similar irrespective of HR. Thus we do not feel the HR affected the residual stress levels, coordination number, etc. around the Tb^{3+} ions. A change in scattering is also not responsible since the HR does not affect grain sizes.

Instead, we feel that the changes in PL intensity can be attributed to changes in oxygen stoichiometry and/or change in the oxidation state of the Tb ions incorporated within the samples caused by low oxygen partial pressure during processing. In another oxide system, Shen and Clarke found exposure to a very low oxygen partial pressure environment causes a decrease in luminescent intensity.[28] In our case, a low oxygen partial associated with CAPAD processing can cause changes in oxidation state of the Tb ions or oxygen reduction of the alumina itself, leading to oxygen vacancies. Tb ions are multivalent and can be Tb^{4+} or Tb^{3+} yet only Tb^{3+} ions cause PL at the wavelengths observed in Figure 6 (485 nm and 543 nm). These PL transitions prove the existence of Tb^{3+} ions in the Tb:Al_2O_3 ceramics, however a varying Tb^{3+} to Tb^{4+} ratio would cause a difference in PL intensity from the samples. As we vary the HR the amount of time the ceramics are exposed to reducing atmospheres also varies. The experiments we conducted with varying holding times (Figure 6c and d) show a similar trend: the longer the exposer time, the lower the PL intensity.

We used X-ray photoelectron spectroscopy (XPS) analysis to examine the local structure around the Tb ion. XPS is a powerful and appropriate technique to determine the local structure of the incorporated Tb ions, such as spin-orbit splitting, binding energies of core levels of the Tb and valence number.[29,30] Although the XPS results (not shown here), clearly revealed the existence of Tb in the samples, unfortunately the analyses was inconclusive with regard to a varying Tb^{3+} to Tb^{4+} ratio. The XPS analysis was complicated because of overlapping of the Tb peaks with the O and/or Al peaks. Further investigations into the cause of the varying PL intensity are underway.

Figure 7 shows the time dependent luminescence of the Tb:Al_2O_3 ceramics produced using a 300 °C min^{-1} and 600 °C min^{-1} HR. Figure 7a and c show the normalized emission vs. times while Figure 7b and d show the luminescent intensities decay on a natural log scale vs. time. For the emission at 485 nm the lifetimes are 750 μs and 680 μs for the Tb:Al_2O_3 ceramics produced using a 300 °C min^{-1} and 600 °C min^{-1} HR, respectively. And for the emission at 543 nm the lifetimes are 720 μs for 300 °C min^{-1} and 670 μs for the 600°C min^{-1} sample. These lifetimes are long and well within the range of lifetimes seen in other luminescent ceramics that are used for laser applications. For example, fluorescence lifetimes of polycrystalline Nd:YAG ceramics used as gain media are typically about 250 μs.[31] The lifetimes of various Tb doped oxides and nitrides have been presented by Chambers and Clarke[19] to be on the order of ~1000 μs, which compares well with the lifetime values presented here for these ceramics. It should be noted that while the HR does effect the PL lifetime, its dependence is not strong. At most there is a ~10% change in the lifetime values as a function of HR. This is markedly different than the effect of HR in PL intensity which causes as much as a fivefold increase in the PL intensity, as discussed above. These results further corroborates that HR does not significantly change the local electronic environment around the luminescent Tb^{3+} ions.

Preliminary thermal characterization of the ceramics via the 3ω-method shows a thermal conductivity of ~30 W m^{-1} K^{-1} at room temperature which is significantly higher than the state of the art gain media. Full thermal characterization studies are underway and will be presented in a subsequent communication. Ceramics that emit in the green and blue wavelengths with high thermal conductivity have the potential to be used in producing substantially higher powered green lasers. This opens the door for producing more compact and stable, higher power green lasers at 543 nm.

3. Conclusion

In summary, we have demonstrated the successful incorporation of above equilibrium concentrations of Tb^{3+} dopant in polycrystalline bulk alumina for the first time. The Tb:Al_2O_3 ceramics show two sharp visible photoluminescent peaks, a blue one centered at 485 nm and a green one at 543 nm. The CAPAD processing conditions namely the sample hold time and heating rate have significant effects on the PL intensity, but do not strongly affect PL lifetimes. Increasing the HR from 150 °C min^{-1} to 600 °C min^{-1} causes an approximate fivefold increase in the PL intensity, yet has a minimal effect on the PL lifetime (a ~10% decrease). The changes in the PL intensity are likely due to changes in the oxygen stoichiometry of the samples as a function of the HR. These results show that it is possible to produce highly transparent light emitting ceramics that are not based on optically isotropic crystal structures. These

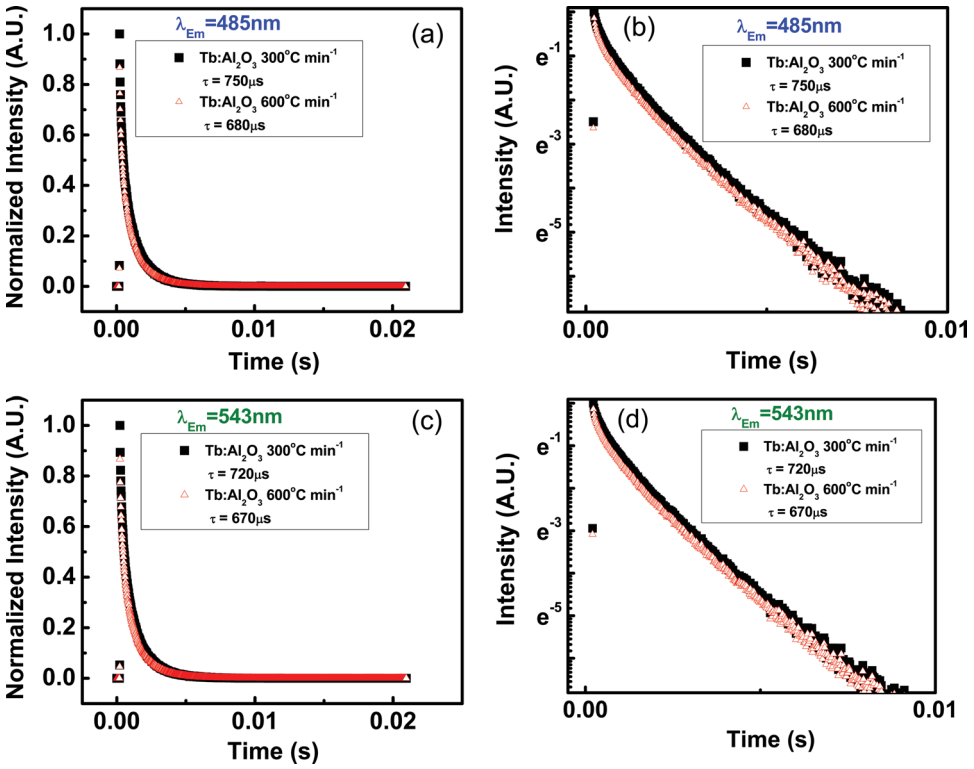

Figure 7. Photoluminescence Lifetime (τ) Curves for the Tb:Al_2O_3 samples produced at 1200 °C, 105 MPa, and with a 10 min hold time for heating rates of 300 °C min^{-1} and 600 °C min^{-1} for the Tb^{3+} ion transitions. The excitation source was a frequency tripled Nd:YAG laser, $\lambda = 355$ nm, operating at 6 ns pulse width. (a) Normalized intensity vs. time for 485 nm ($^5D_4 \rightarrow {}^7F_6$). (b) Natural log intensity vs. time for 485 nm ($^5D_4 \rightarrow\leftarrow {}^7F_6$). (c) Normalized intensity vs. time for 543 nm ($^5D_4 \rightarrow {}^7F_5$). (d) Natural log intensity vs. time for 485 nm ($^5D_4 \rightarrow {}^7F_5$).

findings have great promise for the design of alumina-based light producing devices and should be especially interesting for the continued development of high-powered lasers.

4. Experimental Section

Powder Preparation: Commercially available aluminum oxide, α-Al_2O_3 (99.99% purity, TM-DAR, Taimei Chemicals, Japan) was processed as received (referred to as un-doped) as well as doped with Terbium Oxide, Tb_4O_7 (99.9% purity, Nanostructured & Amorphous Materials, Inc., USA). The powders were weighed to achieve a Tb doping level of 0.5 at%. The powders were mixed for 12 h by ball milling in a glass container. Ultra-High Purity (99.99% purity) water was used as a dispersant at a ratio of 10 grams total powder to 200 mL of UHP water. Alumina balls (99.9% density and purity, Performance Ceramics Co., Penninsula, OH, USA) with a 5 mm diameter were selected for the milling media, at a 1:15 powder:ball weight ratio. After milling the powders were sieved to separate them from the milling media, then dried in air at 120 °C for 12h in a furnace.

CAPAD Processing: The as received alumina powder and the as mixed Tb:Al_2O_3 powders were densified and processed using the CAPAD technique. In all cases, 1.2500 g ± 0.0001 g of powder was poured into a graphite die with an inner diameter of 19 mm and secured between two graphite punches of the same outer diameter. The die, plunger, and powder set were placed into the CAPAD and secured between two graphite spacers and copper electrodes. A maximum vacuum of 1×10^{-3} Torr was achieved in all cases. A custom constructed CAPAD apparatus that has been described previously[6] was used. Briefly, the CAPAD consists of a vacuum chamber, within which an electrode set has been inserted and are all contained within a load cell controlled twin ball screw H-frame Instron mechanical testing system.

The powder was pre-pressed at 70 MPa for 1 min in order to create a green body. Simultaneously with the subsequently mentioned heating parameters, the green pellet was subjected to an applied compressive load, which was linearly increased to its maximum value of 105 MPa over a time interval of 3 minutes and held constant throughout until sample processing was completed, whereby the load was released. We used DC power supplies (Model XDC 10–1200, Xantrex, Burnaby, B.C., Canada), with which the samples are brought to and maintained at temperature via joule heating of the graphite plunger and die assembly. The sample temperatures are measured with an optical pyrometer (Model IR GAP, Chino, Torrance, CA, USA), focused on a hole drilled in the graphite die located at the center point of the die height. This location was chosen as it has been found previously[32,33] to best represent the true sample temperature during CAPAD processing.

Samples were produced at temperatures ranging between 700–1200 °C with a 10 min holding time (HT) at temperature with a 300 °C min^{-1} heating rate (HR) in order to determine the effect of temperature on the resultant sample density and transparency.

Since it was found that the highest density and best optical quality was obtained at 1200 °C, we also produced samples at this temperature with various HR's (150 °C min^{-1}, 300 °C min^{-1}, and 600 °C min^{-1}) in order to study the effects of HR on the resultant sample transparency and photoluminescence properties. Since samples produced at different HR's reach the maximum sample temperature at different times, this means that the total experiment times (TET) are also varied when the HR is varied and the HT is maintained constant. Therefore, in order to de-couple the effects of HR and HT samples were produced at the three HR mentioned above, with the HT held constant at 10 min and then with the HR held constant at 300 °C min^{-1} and the HT varied at 10 min, 20 min, and 30 min. In all cases the maximum achieved temperature was 1200 °C.

Microstructural Characterization: The AGS of the undoped densified and reaction densified ceramics were obtained by measuring

approximately 500 grains over multiple scanning electron micrographs of fracture surfaces using the ImageJ software. In addition to the AGS, a statistical standard deviation of the measured grains was calculated from the AGS measurements. All images were acquired using a Phillips XL30 Field Emission Scanning Electron Microscope (FE-SEM) with secondary electron detection. Prior to SEM the fracture surfaces were coated with a monolayer of platinum palladium using a Cressington 208 sample preparation system. The sputtering lasted for 10 sec at a target to sample distance of 3.75 cm.

UV-VIS-IR Transmission Measurements: Optical Transmission spectra were taken on a Varian Cary 50 UV-VIS spectrometer from 275 nm to 1050 nm. The bulk polished samples were placed at normal incidence to the beam path. The scans were obtained at a rate of 0.2 nm s^{-1}.

Photoluminescence Measurements: Photoluminescence data were taken on a Horiba Spex Fluorolog 3 Spectrophotometer system using a tungsten deuterium lamp with monochromators as a light source. All measurements were taken in front face mode on polished bulk samples. Excitation scans were taken between λ = 275 nm and λ = 430 nm while monitoring the sample emission at λ_{Em} = 485 nm, allowing the determination of the pumping bands. Emission scans were taken between λ = 465 nm and λ = 560 nm with the pumping wavelength λ_p = 285 nm as it was determined to be an effective pumping wavelength from the excitation spectra. All measurements were taken with an integration time of 1s per nanometer.

Photoluminescence Lifetime Measurements: The PL Lifetimes (τ) were taken by irradiating the samples with a frequency tripled Nd:YAG laser, λ = 355 nm operating at 6 ns pulse width. The emission intensity was measured with a photodiode and captured with an oscilloscope. A double exponential fit[19] of the resulting curves was used to extract the PL lifetime, whereas the lifetime is defined as the time required for the output signal intensity to decrease by a factor of 1/*e*.

Acknowledgments

The funding of this work from the Army Research Office (ARO) and the High Energy Laser – Joint Technology Office (HEL-JTO) is gratefully acknowledged. We thank Dr. P. Martinez-Torres for assistance and discussion with the PL measurement and analysis and Mr. C. Hardin and Dr. D. Evans for help with lifetime measurements.

Received: March 13, 2013
Published online: August 8, 2013

[1] R. L. Coble, *Transparent Alumina and Method of Preparation* **1962**, US Patent 3026210.
[2] W. H. Rhodes, D. J. Sellers, T. Vasilos, *J. Am. Ceram. Soc.* **1974**, *58*, 31–34.
[3] A. Ikesue, Y. L. Aung, *Nature Photonics* **2008**, *2*, 721–727.
[4] A. Ikesue, Y. L. Aung, T. Yoda, S. Nakayama, T. Kamimura, *Optical Mater.* **2007**, *29*, 1289–1294.
[5] A. Ikesue, *Optical Mater.* **2002**, *19*, 183–187.
[6] J. E. Garay, *Annu. Rev. Mater. Res.* **2010**, *40*, 445–468.
[7] M. O. Ramirez, J. Wisdom, H. Li, Y. L. Aung, J. Stitt, G. L. Messing, V. Dierolf, Z. Liu, A. Ikesue, R. L. Byer, V. Gopalan, *Optics Express* **2008**, *16*, 5965–73.
[8] L. D. Merkle, M. Dubinskii, K. L. Schepler, S. M. Hegde, *Optics Express* **2006**, *14*, 3893–905.
[9] I. Shoji, T. Taira, A. Ikesue, *Optical Mater.* **2007**, *29*, 1271–1276.
[10] W. Yi, S. Xudong, Q. Guanming, *J. Rare Earths* **2007**, *25*, 68–71.
[11] J. Kong, J. Lu, K. Takaichi, T. Uematsu, K. Ueda, D. Y. Tang, D. Y. Shen, H. Yagi, T. Yanagitani, A. A. Kaminskii, *Appl. Phys. Lett.* **2003**, *82*, 2556.
[12] N. P. Padture, P. G. Klemens, *J. Am. Ceram. Soc.* **1997**, *20*, 1018–1020.
[13] P. H. Klein, *J. Appl. Phys.* **1967**, *38*, 1603.
[14] L. D. Merkle, N. Ter-Gabrielyan, *J. Luminescence* **2013**, *133*, 254–256.
[15] C. Gheorghe, A. Lupei, V. Lupei, A. Ikesue, M. Enculescu, *Optical Mater.* **2011**, *33*, 501–505.
[16] R. Berman, E. L. Foster, J. M. Ziman, *Proc. Roy. Soc. A* **1955**, *231*, 130–144.
[17] A. Krell, K. Waetzig, J. Klimke, *J. European Ceram. Soc.* **2012**, *32*, 2887–2898.
[18] R. Apetz, M. P. B. Bruggen, *J. Am. Ceram. Soc.* **2003**, *86*, 480–486.
[19] M. D. Chambers, D. R. Clarke, *Annu. Rev. Mater. Res.* **2009**, *39*, 325–359.
[20] T. H. Maiman, *Nature* **1960**, *187*, 493–494.
[21] R. Kumaran, S. E. Webster, S. Penson, W. Li, T. Tiedje, P. Wei, F. Schiettekatte, *Optics Lett.* **2009**, *34*, 3358–60.
[22] A. Krell, G. M. Baur, C. Dahne, *Proc. SPIE* **2003**, 199–207.
[23] A. Ikesue, K. Yoshida, *J. Mater. Sci.* **1999**, *34*, 1189–1195.
[24] E. H. Penilla, Y. Kodera, J. E. Garay, *Mater. Sci. Engineering B* **2012**, *177*, 1178–1187.
[25] C. Pecharromán, G. Mata-Osoro, L. A. Díaz, R. Torrecillas, J. S. Moya, *Optics Express* **2009**, *17*, 6899–912.
[26] G. H. Dieke, *Spectra and Energy Levels of Rare Earth Ions in Crystals*, Interscience, New York **1968**.
[27] A. Krell, A. Teresiak, D. Schläfer, *J. European Ceram. Soc.* **1996**, *16*, 803–811.
[28] Y. Shen, D. R. Clarke, *J. Am. Ceram. Soc.* **2009**, *92*, 125–129.
[29] B. D. Padalia, W. C. Lang, P. R. Norris, L. M. Watson, D. J. Fabian, *Proc. R. Soc. London A* **1977**, *354*, 269–290.
[30] C.-C. Lin, Y.-P. Chang, H.-B. Lin, C.-H. Lin, *Nanoscale Res. Lett.* **2012**, *7*, 187.
[31] A. Ikesue, Y. L. Aung, T. Taira, T. Kamimura, K. Yoshida, G. L. Messing, *Annu. Rev. Mater. Res.* **2006**, *36*, 397–429.
[32] X. Wang, S. R. Casolco, G. Xu, J. E. Garay, *Acta Mater.* **2007**, *55*, 3611–3622.
[33] U. Anselmi-Tamburini, S. Gennari, J. E. Garay, Z. a. Munir, *Mater. Sci. Engineering A* **2005**, *394*, 139–148.